Eur. Phys. J. B **60**, 171–179 (2007)
DOI: 10.1140/epjb/e2007-00342-9

THE EUROPEAN PHYSICAL JOURNAL B

Dispersion and thermal resistivity in silicon nanofilms by molecular dynamics

P. Heino[a]

Tampere University of Technology, Institute of Electronics, P.O. Box 692, 33101 Tampere, Finland

Received 27 August 2007 / Received in final form 23 October 2007
Published online 8 December 2007 –

Abstract. On nanoscale, thermal conduction is affected by system size. The reasons are increased phonon scattering and changes in phonon group velocity. In this paper, the in-plane thermal resistivity of nanoscale silicon thin films is analyzed by molecular dynamics (MD) techniques. Modifications to the dispersion relation are calculated directly with MD methods at high temperature. The results indicate that the dispersion relation starts to change for very thin films, at around two nanometers. The reasons are band folding and phonon confinement. Thermal resistivity is analyzed by the direct non-equilibrium method, and the results are compared to kinetic theory with modified dispersion relations. Thermal resistivity is affected by both surface scattering and dispersion. Moreover, in thin films, the characteristic vibrational frequency decreases, which in standard anharmonic scattering models indicates a longer relaxation time and affects the resistivity. The results indicate that in very thin films, the resistivity becomes highly anisotropic due to differences in surface scattering. In two cases, surface scattering was found to be the most important mechanism for increasing thermal resistivity, while in one case, phonon confinement was found to increase resistivity more than surface scattering.

PACS. 63.22.-m – 31.15.Qg Molecular dynamics and other numerical methods – 65.80.+n Thermal properties of small particles, nanocrystals, and nanotubes

1 Introduction

Nanoscale features are routinely processed in the electronics industry today. Increasing performance and decreasing feature size have raised the issue of thermal design in such devices. On this length scale, the size is comparable to the mean free path of heat carriers, and thermal properties are affected by the system size. On macroscale, thermal energy transfer is calculated with the *phenomenological* Fourier law derived in the early 1800's [1], which treats thermal conductivity as a material property. However, on micro and nanoscales, the Fourier equation breaks down in the sense that heat flux and thermal gradient cannot be related with a parameter that depends only on the material. On these length scales, thermal conductance also depends on size and microstructure of the system. These microscale properties increase the scattering rate of heat carriers, and therefore increase thermal resistance. Moreover, on nanoscale, the structure affects the phonon modes and their velocities, which also affect the resistance. Therefore, micro- and nanoscale thermal conduction has attracted a lot of interest in the past two decades [2–5].

On small length scales, when the system size is some mean free paths, thermal conduction can be calculated with the Boltzmann transport equation (BTE) [3]. The solution of BTE falls into three classes: directly solving the BTE as a partial differential equation [6], using direct phonon simulation techniques such as Monte Carlo [7–9] or lattice Boltzmann [10] to obtain the solution, or using results from radiative heat transfer [11]. In the BTE approach, the physics of heat transfer, dispersion, and phonon scattering are incorporated explicitly to the calculations. Thus, for reliable calculation, a good understanding of the fundamental phonon processes and relaxation times is required. For some phonon processes, such as point defects, impurities, or boundaries, fairly accurate relaxation time models are available [12]. However, for some more complicated processes, such as interfaces, such information is not available [2].

In addition to BTE, the molecular dynamics (MD) method has become a tool for studying thermal conduction on the nanoscale [4,5,13]. With MD, the thermal conductivity can be calculated from equilibrium calculations, from a known heat flux and temperature gradient [13], or from temperature decay calculations [14]. It is best suited for studying the effect of structural imperfections (boundaries, dislocations, grain boundaries, voids, interstitials, etc.) on thermal conductivity. It should be emphasized that even if conductivity on the nanoscale is *not* a property of the *material*, one can calculate a heat flux and a temperature gradient, and call their ratio the conductivity.

[a] e-mail: pekka.heino@tut.fi

The main limitations of MD are the very limited size and time scales that can be studied. Typically the maximum size scale can be a few hundred nanometers (a few mean free paths), and the time scale only some nanoseconds. Moreover, the role of electrons can not studied, and an accurate interaction between atoms may be hard to find.

The applicability of these models is somewhat different. Considering the size scale, the phonon models are applicable only if one can speak about phonons as particles. Therefore, the size scale should be larger than the phonon wavelength and the wavepacket size [15]. As MD describes the motion of the atoms, the lower size limit is of the order of the lattice constant [10]. Since the displacements of the atoms form the waves, the interatomic distance is less than the phonon wavelength [15]. As for the temperature, the MD simulation is classical, and cannot therefore describe the low-temperature distribution of phonons. However, at high temperatures the distributions are equal, and MD is applicable, when the temperature exceeds the Debye temperature [16]. At room temperature, the typical phonon wavelength is around 1–2 nm, [4] [p. 182] and the mean free path in silicon is around 30–200 nm depending on the phonon mode and frequency [16].

As the molecular dynamics method is a more fundamental approach to lattice vibrations than the BTE, the results of an MD simulation can provide the necessary data for BTE simulations. Scattering processes and relaxation times have been much studied by MD [17–22]. However, modifications to the dispersion relation due to size effects have not been studied by MD in thin films. Dispersion in nanotubes has been studied. Mingo [23] used an approximate potential to calculate dispersion in silicon nanotubes, and used it for analytical conductivity studies. Shiomi and Maruyama [24] studied thermal conduction in carbon nanotubes and used the full dispersion curve in their analysis. It is noted that in the context of continuum elasticity, many authors have have studied phonon confinement and/or its effect on thermal conduction [25–29]. However, in the context of continuum elasticity, the wavelength must be much larger than the interatomic spacing, and therefore the analysis is applicable only at very low temperatures. Moreover, the elastic models used in these calculations are isotropic, and therefore the calculations are only approximate for crystalline materials.

The purpose of this paper is to study the finite size effect on the dispersion relation in nanoscale silicon thin films by MD simulations. The effect on thermal resistivity is analyzed by kinetic theory, and the results are compared to non-equilibrium MD results. The interaction between silicon atoms is described with the modified embedded atom (MEAM) potential. In addition, the dispersion curves for solid argon are computed to serve as a validity check for the methods used. In contrast to the continuum approach, MD simulations for silicon are carried out at high temperatures, where the typical phonon wavelength is only a few lattice constants. Moreover, the MD model is naturally anisotropic.

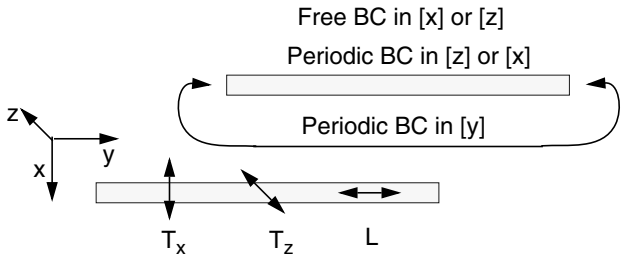

Fig. 1. Description of the boundary conditions (BC) used in the thin film simulations. Free boundaries are applied in one transverse direction (T_x or T_z), while periodic boundaries are applied in the other two directions. The longitudinal (L) phonons are parallel to y.

2 Simulations

The simulations of this paper consist of two parts: dispersion relations and thermal resistance. Dispersion relations are calculated both for bulk silicon systems and thin films. In addition, the bulk dispersion relation for solid argon is calculated to serve as a validity check for the methods and models used. The interaction between argon atoms is described with the Lennard-Jones potential, as discussed e.g. in reference [30]. The silicon system is described with the potential based on the modified embedded atom method (MEAM), as developed by Baskes [31].

2.1 Dispersion relation

The dispersion relation can be calculated from the velocity-velocity autocorrelation function. In this work, the dispersion relation is calculated as described by Papanicolau et al. [32] Specifically, the vibrational spectrum for a given wavevector, k, is calculated as the Fourier transform of the autocorrelation function. For a given polarization, $p = x, y, z$, the autocorrelation function is defined as:

$$A^p(k,t) = \frac{\langle \nu_k^p(0)\nu_k^p(t)\rangle}{\sum_p \langle \nu_k^p(0)\nu_k^p(0)\rangle}, \tag{1}$$

$$\nu_k^p(t) = \sum_i v_i^p(t) e^{-ik\cdot r_i(t)}. \tag{2}$$

Here k is the wavevector of interest, v_i^p the p component of the velocity of atom i, and r_i the position of atom i. As such, $\nu_k^p(t)$ is the reciprocal space representation of the velocity and $A^p(k,t)$ its autocorrelation. By Fourier transforming $A^p(k,t)$, the eigenfrequencies for a given wavevector k and the corresponding amplitudes can be found. Typically sharp peaks are found, and the dispersion relation is determined from the locations of these peaks.

For the bulk dispersion relation periodic boundaries are used in all directions. The system size in the direction of the wavevector is 10 nm, in the other directions about 4 nm. Even if the size of the system limits the maximum phonon wavelength, the bulk dispersion relation was independent of system size for this system and also for a system of half this size with periodic boundaries. To obtain

the dispersion relation in different wavevector directions, different crystal orientations are used. The wavevector is always aligned along the y-direction, and the crystal orientations used are $y[100]$, $x[010]$, $z[00\bar{1}]$; $y[110]$, $x[001]$, $z[\bar{1}10]$; and $y[111]$, $x[\bar{1}10]$, $z[11\bar{2}]$. The system size and the lattice constant determine the values of k that can be used in the calculations: the wavelength, $\lambda = 2\pi/k$, cannot exceed the system size, and it must be at least two nearest neighbor distances, so that a reasonable wave can be described. The system size, as stated above, is around 20 lattice constants, i.e. about 80 nearest neighbor distances in silicon, in the [100] direction. For comparison, the typical frequency for a phonon is $h\nu = k_B T$ (Tien et al. [3], p. 24), which for silicon yields a typical phonon wavelength of $\lambda = (hv)/(k_B T) = 1$ nm at the temperature $T = 300$ K ($v = 6500$ m/s [13]). This is ten times smaller than the system size in the direction of k. When thin films are studied, one of the two directions perpendicular to the wavevector is described with free boundaries. The film thickness is varied between a few atomic layers and 4 nm. As an alternative to free boundaries, fixed film boundaries could also be used. However, in real structures, the thin films are most likely connected to other films. These boundaries are not often mechanically stiff [33], and therefore free boundaries are used instead of fixed boundaries. The simulation setup for the thin film systems is shown in Figure 1. For bulk systems, the boundaries are periodic in all directions.

Initially the system was thermalized to a thermal equilibrium by applying the Nosé-Hoover thermostat at a given temperature for 100 000 time steps. For solid argon, the temperatures 10 K and 82 K were chosen, as motivated by the experiments of Fuji et al. [34] For silicon, the room temperature, 300 K, was chosen for practical interest. The time step 3 fs was chosen as it was the largest time step that could conserve the total energy in NVE calculations. After thermalization, the simulations were run for half a million time steps to obtain the dispersion relation. The value of $\nu_k^p(t)$ was stored for all k at every fourth time step. This sampling rate could still capture the highest frequencies present in the system. A higher sampling rate would require more data storage, but would not reveal any new vibrational properties. The dispersion relation is of great importance in nanoscale thermal conduction problems, as it defines the group velocity of heat carriers.

2.2 Thermal resistivity

Thermal resistance can be calculated with MD using equilibrium or non-equilibrium techniques [13]. In equilibrium methods, thermal conduction is calculated from the heat flux autocorrelation function in a thermal equilibrium. In one of the non-equilibrium methods, a temperature gradient and a heat flux are imposed on the system, and thermal resistivity is calculated from their ratio. In principle, either the heat flux or the temperature gradient is given, and the other is computed from a stationary state using MD techniques. Temperature is calculated as a spatio-temporal average in the stationary state. Usually the system is divided into layers, and the temperature of each layer is calculated by averaging. In this work, a constant heat flux was used, as proposed by Jund and Jullien [35]. The method has been frequently used, and the author has also used it previously to compute the thermal conductivity of bulk silicon, described with the present potential [36].

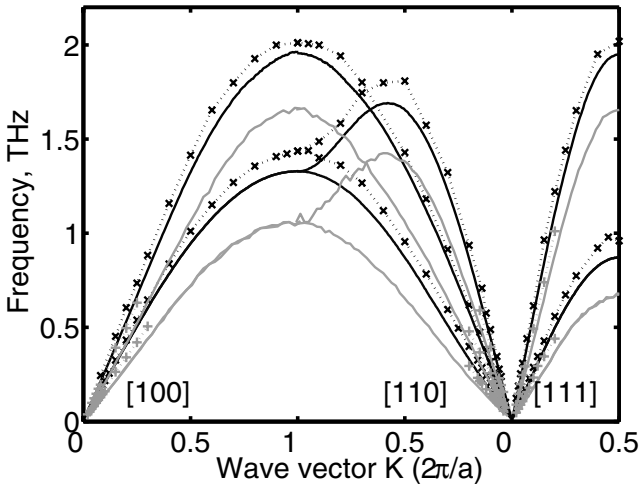

Fig. 2. Dispersion relation of solid argon. The solid lines are from the MD simulations with the Lennard-Jones potential. The crosses and dotted line are from the experiments by Fuji et al. [34]. The black lines represent the longitudinal modes and the grey lines the transverse modes. The higher frequencies are measured/calculated at 10 K and the lower frequencies are measured/calculated at 82 K.

In this work, the thermal resistivity was calculated from simulations running a million time steps. The stationary state was already reached after no more than 2×10^5 time steps. Temperature was calculated as a spatio-temporal average of the kinetic energy of the atoms over at least 8×10^5 time steps. For spatial averaging the temperature for each atom layer was calculated separately.

3 Results

3.1 Dispersion relation for bulk systems

The dispersion relations, as calculated from the autocorrelation function (Eqs. (1) and (2)) are shown in Figure 2 for bulk solid argon. For comparison, the experimental data has been included in the figure. Since experimental data is available for a low and a high temperature, the dispersion relation has been calculated at these temperatures. This figure shows that the MD method can reproduce the dispersion relation with good accuracy if the interatomic potential is chosen correctly. It should be emphasized that in contrast to the use of the dynamical matrix, MD can also be used at finite temperatures as it naturally takes into account the anharmonic effects and thermal expansion [37].

Silicon was described with the modified embedded atom method (MEAM), as described by Baskes [38]. For

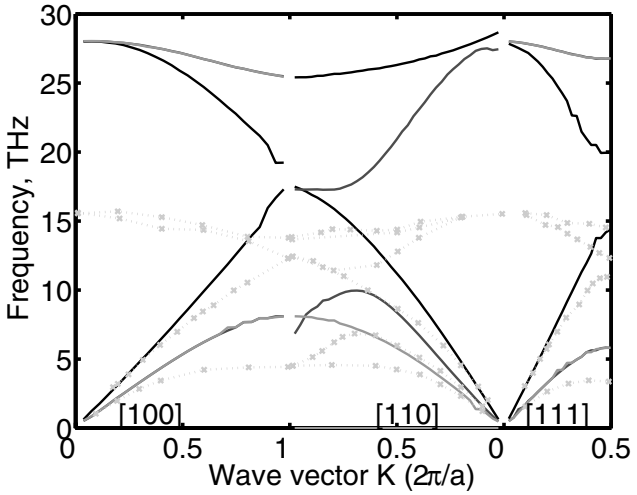

Fig. 3. Dispersion relation of silicon, as calculated with the MEAM potential at 300 K. The solid lines are from simulations, the crosses and the dotted line from the work of Flensburg and Stewart [40].

the parameterization of the potential, the reader is referred to the earlier work [31]. The potential was chosen since it has a relatively long range of interaction, and therefore the energy of free surfaces will be accurately described. This is in contrast to the Stillinger-Weber and Tersoff potentials that are only first neighbor models, and therefore cannot describe surface relaxations and may become inaccurate near surfaces. In the case of thin films with free boundaries, the surface properties in particular are very important. Baskes [39] has used the MEAM potential for silicon surfaces.

The dispersion relation for bulk MEAM silicon is shown in Figure 3. From the figure it can be seen that the frequencies of only the long acoustic phonons are reproduced with reasonable accuracy. Qualitatively the forms are similar, but the frequency increases too fast with increasing wavevector. For the optical modes, the frequency is far too high. This shows that the potential for the nearest neighbor interaction is too stiff. However, as seen from the reference data, the group velocity of optical phonons in silicon is much lower than that of the acoustic phonons. Therefore, for heat conduction, the acoustic phonons are much more important than the optical phonons. Moreover, the anharmonic scattering rate has a strong frequency dependence, so that most thermal energy is carried by low frequency phonons. Therefore, for thermal conduction simulations the inaccuracy of the high frequency phonons does not necessarily mean inaccurate results.

3.2 Dispersion relation for thin films

To study the effect of the free surfaces on the dispersion relation, thin silicon films with different crystal orientations were studied. The crystal orientations and the free surface directions are shown in Figure 1. As in the case of the bulk simulations, the wavevector is always aligned

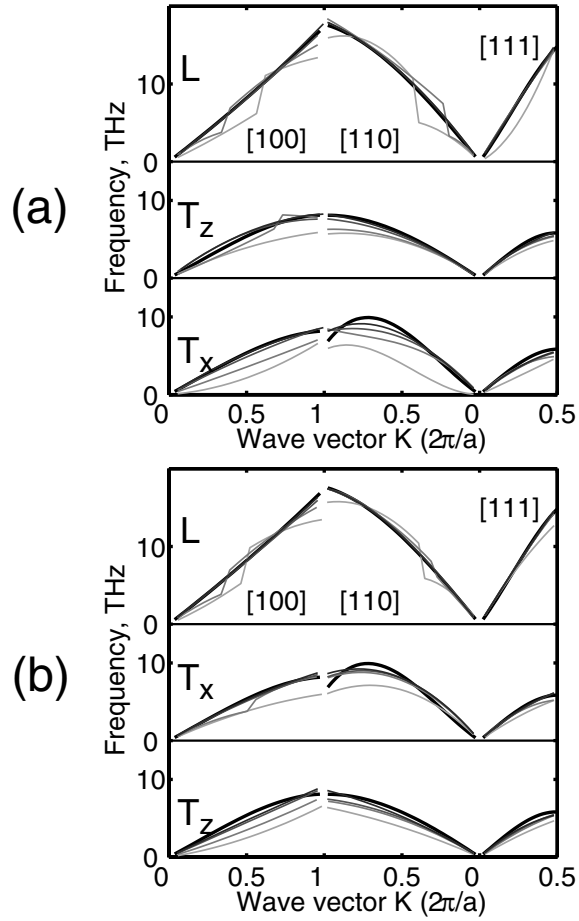

Fig. 4. Dispersion in thin silicon films with free boundaries in one direction. In (a) the free boundary is perpendicular to the x-direction, and in (b) perpendicular to z. The thick, black line is the bulk relation, and the thin lines are dispersion relations for films of thicknesses 3, 6, 10, and 14 atomic layers. For the largest systems, the deviation from the bulk results is minor. In both figures the transverse vibrations perpendicular to the free surface are shown in the lowest part.

in the y-direction, and the crystal orientations are $y[100]$, $x[010]$, $z[00\bar{1}]$; $y[110]$, $x[001]$, $z[\bar{1}10]$; and $y[111]$, $x[\bar{1}10]$, $z[11\bar{2}]$.

The dispersion curves for MEAM silicon were calculated in films consisting of 3, 4, 5, 6, 8, 10, 12, and 14 atomic layers. The thickness of the largest systems is around 25 Å. Some of these results are shown in Figure 4. The results for intermediate size are similar, and are omitted for the sake of clarity. The results for the largest systems differ only a little from the bulk results, since the surface atoms play only a minor role in large systems.

As discussed above, the dispersion relations are obtained from the peaks of the Fourier-transformed velocity-velocity autocorrelation function, i.e. vibration spectrum. In bulk systems this procedure gives well defined peaks for the transverse and longitudinal, optical and acoustic phonons, as shown in Figures 2 and 3. However, in the case of thin films, the phonons have multiple discrete modes, as discussed in the context of continuum models [25,29].

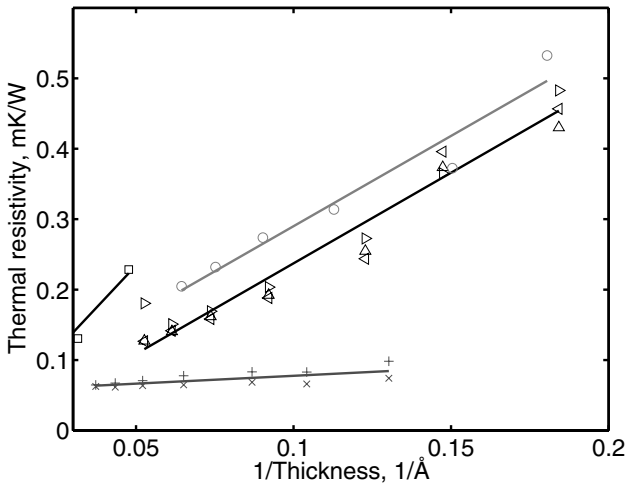

Fig. 5. Thermal resistivity of silicon thin films as calculated with the direct non-equilibrium method. The resistivity values are very high compared to the experimental value due to small system size. Three different free surfaces are present in the six simulation cases: (100) triangles, $(\bar{1}10)$ crosses, and $(11\bar{2})$ circles. The square marks are results from similar calculations by Li and Xiao [41] with the Stillinger-Weber potential. The lines are best fits to the data.

In the MD simulations, the vibration spectrum may show multiple peaks for a given wavevector. In practice, as compared to the bulk simulation, the peaks seem to split into at most three visible peaks. This can be taken as evidence of phonon confinement in the MD simulations. From these peaks, only the most significant one is recorded. Figure 4 shows a discontinuous jump, when the most significant mode changes. In Figure 4, none of the systems with ten or more atomic layers contained discontinuous points in the dispersion relation. Therefore, this kind of discrete behavior is seen only in very thin films, around 1.5 nm or less, and only for some crystal orientations. It it possible that in other cases the finite temperature induces too much broadening to the vibrational spectra, and confinement is not seen, even if discrete modes were present. As seen in the figure, when confinement effects are seen, the group velocity can change significantly. Numerical differentiation of the dispersion curves gives the reduction by a factor of at most two.

3.3 Thermal resistivity of silicon thin films

Thermal resistivities of the silicon films were also calculated with the direct non-equilibrium MD method, as discussed above. The simulation was done for the same systems as the thin film dispersion calculations, and the crystal orientations were given above. These simulations result in three cases with a free (100) surface, two cases with a free $(\bar{1}10)$ surface, and one case with a free $(11\bar{2})$ surface. The results are shown in Figure 5. For the sake of comparison, some results from the simulations of Li and Xiao [41] with the Stillinger-Weber potential are included in the figure. The free (100) surfaces are indicated by triangles, $(\bar{1}10)$ surfaces by crosses, and the$(11\bar{2})$ surface by circles.

The results clearly show two different dependencies on the size. In the case of free (100) and $(11\bar{2})$ surfaces, the thermal resistivity is heavily dependent on the film thickness, while in the case of $(\bar{1}10)$ surface, the results are not so heavily dependent on the thickness, and the conductivity is also much better.

4 Discussion

4.1 Conductivity by kinetic theory

Kinetic theory is a well defined framework to study thermal conduction by phonons. In that context, the thermal conductivity of a phonon system is (e.g. Dames and Chen [42]):

$$\kappa = \frac{1}{3}\int C(\omega)v_g(\omega)\Lambda(\omega)d\omega. \tag{3}$$

As the group velocity of optical phonons is very low, and the frequency high (meaning a high scattering rate), the optical phonons are often excluded from the analysis. When the optical modes are excluded, the conductivity comes from the three acoustic modes, m, and the conductivity can be written as:

$$\kappa = \frac{1}{3}\sum_m \int C_m(\omega)v_{g,m}(\omega)\Lambda_m(\omega)d\omega. \tag{4}$$

This equation consists of three terms: the heat capacity of the mode, $C_m(\omega)$, the group velocity, $v_{g,m}(\omega)$, and the mean free path $\Lambda_m(\omega)$. All these depend on the mode and frequency, and will be discussed below.

For the heat capacity of a mode, consider the energy of a mode, $E_m = \hbar\omega \int n(\omega)g(\omega)d\omega$. By definition, the heat capacity is $C_m = \partial E_m/\partial T$. As the density of states is not heavily dependent on the temperature, e.g. in the Debye and Einstein approximations it is independent [3] (p. 22), heat capacity becomes $C_m(\omega) = \hbar\omega g(\omega)\partial n/\partial T$. In a real, quantum mechanical solid, the distribution function is the Bose-Einstein distribution $(\exp(\hbar\omega/k_BT) - 1)^{-1}$. However, as the molecular dynamics calculations are classical, the distribution function becomes $n(\omega) = k_BT/\hbar\omega$ [43], which is exactly the high temperature approximation of the Bose-Einstein distribution [3] (p. 50). Therefore, the heat capacity of a mode becomes $C_m(\omega) = k_Bg(\omega)$. As pointed out by Schelling et al. [13], the heat capacity in equation (3) is intended to be only for those modes that carry heat. As silicon has both optical and acoustic phonons, of which only the acoustic phonons carry heat significantly, the total heat capacity of the system to be used in MD simulations is $3k_Bn/2$. The means that the heat capacity of a mode should be $k_B/2$. This condition was used to properly normalize $C_m(\omega)$.

The group velocity is, by definition:

$$v_g = \frac{\partial\omega}{\partial k}, \tag{5}$$

and is calculated from the simulated dispersion curves. When present, non-differentiable points are excluded from the velocity calculations.

The mean free path, $\Lambda = v_g\tau$, is affected by different phonon scattering processes and their relaxation times, τ. In bulk crystals, the important scattering mechanisms are the anharmonic scattering and the impurity scattering [23]. However, as the MD system does not contain any impurities, anharmonic scattering can be considered to be responsible for the scattering in bulk silicon MD simulations [44]. The anharmonic terms are different for longitudinal and transverse modes [12], and they can be expressed as:

$$\tau_L^{-1}(\omega) = A_L T^{\chi_L}\omega^{\xi_L} e^{-B_L/T} \quad (6)$$

$$\tau_T^{-1}(\omega) = A_T T^{\chi_T}\omega^{\xi_T} e^{-B_T/T}. \quad (7)$$

Here the subscripts T and L refer to the transverse and longitudinal modes.

In addition to anharmonic scattering, in NEMD simulations two other scattering processes can be considered. In simulations with periodic boundaries in all directions, the effective mean free path related to scattering at the heat source and heat sink is $L_y/4$, where L_y is twice the distance between a hot and a cold spot, i.e. the system length in this direction [13]. Factor 4 has been used in numerous studies [15], and may result from scattering at the boundaries between thermostated and unthermostated regions [45]. As there is some uncertainty in the actual value, a MFP of $\beta L/4$ was considered for this scattering. It is also noted that as the length was not varied in these simulations, the parameter β only increases or decreases the thermal resistance, and does not affect the scaling properties related to film thickness.

In addition to heat source scattering, the boundary scattering process is expected to play a major role in thin films. The boundary scattering can be assumed to have a mean free path of αL_x, where L_x is the system thickness and α a factor determining the specular scattering probability s: $\alpha = 1/(1-s)$ [44]. In a system with free boundaries, this scattering process must be included in the calculation of the MFP. In principle, both scattering process parameters α and β could depend on the phonon frequency. However, in that case their estimation would need quite different procedures, preferably direct observation of wavepacket scattering on interfaces [46].

Combining these scattering mechanisms and relaxation times with the Matthiessen rule, the effective MFP and its dependence on frequency can be obtained:

$$\frac{1}{\Lambda_{\mathit{eff}}(\omega)} = \frac{1}{v_g(\omega)\tau_{L,T}(\omega)} + \frac{4}{\beta L_y} + \frac{1}{\alpha L_x}. \quad (8)$$

By combining equations (4) and (8), the dependence of the resistivity on the film thickness and scattering parameters can be found. It is noted that in this context, equation (4) includes anisotropy, since only one longitudinal and two transverse phonon modes are included in the calculations, and their velocities depend on the crystal orientation of the modes. The parameters for longitudinal phonon scattering were taken from the work of Mingo [23] and are: $A_L = 1.73 \times 10^{-19}$ s/K, $B_L = 137.3$ K, $\chi_L = 1$, and $\xi_L = 2$. Transverse phonon scattering is generally not as heavily dependent on the frequency, as the dependence is typically linear [12]. The parameters for transverse phonon scattering were taken from the work of Chantrenne et al. [47] and are: $A_T = 7 \times 10^{-13}$ s/K, $B_T = 0$ K, $\chi_T = 1$, and $\xi_T = 4$. Therefore, the unknowns in the thermal resistivity are the specularity parameter α, and the size parameter β. It has been found, that surface scattering in many cases can be described as diffusive [8,23]

For bulk systems, i.e. when both surface and system size scattering rates are omitted, and the *calculated* vibration spectra and dispersion relations for *bulk* silicon are used, the procedure gives the direction dependent thermal conductivities 138 W/mK [100], 108 W/mK [110], and 175 W/mK [111]. The anisotropy in these cases comes from the different acoustic phonon group velocities in different directions. The average of these values is 140 W/mK, which is reasonably close to the experimental value 150 W/mK. It should be noted that the scattering parameters, as given above, are obtained by fitting MD simulation data (silicon described by the Stillinger-Weber potential) to experimental data. Therefore this agreement suggests only that scattering and group velocity of relevant phonons in the MEAM model are reasonably similar to the SW model. Moreover, the calculations in this work seem to have been performed correctly.

Similarly, one can calculate the predictions for the thermal resistivity, $1/\kappa$, of thin films for various scattering probabilities, thicknesses, and crystal orientations by using the calculated dispersion curves and vibration spectra for the specific case. Moreover, the boundary scattering parameters can be optimized so that the predictions of equation (4) will best reflect the simulated data of Figure 5.

4.2 Surface scattering

As discussed above, the kinetic theory expression has two free parameters that can be tuned to fit the NEMD results of thermal resistivity. This procedure yields information about the directional dependence of the boundary scattering process in silicon nanofilms. When the scattering parameter has been optimized, the thermal resistivities can be presented as a function of film thickness. This is shown in Figure 6. The scattering parameters α used in Figure 6 are 4.52 for (100) surfaces, 60.1 for $(\bar{1}10)$ surfaces, and 2.15 for $(\bar{1}\bar{1}2)$ surfaces. Therefore, the specular scattering probabilities for the (100) and $(\bar{1}\bar{1}2)$ surfaces are significantly lower than for the $(\bar{1}10)$ surface. By calculating the specular scattering probability $s = 1 - 1/\alpha$, the results predict a specular scattering probability of 54% for the $(\bar{1}\bar{1}2)$ surface, 78% for the (100) surfaces and 98% for the $(\bar{1}10)$ surfaces. The last scattering probability is extremely high, indicating almost specular scattering. In all these cases the size parameter β was as high as 10, indicating that on the average, the phonons undergo only one diffuse scattering event when traveling 2.5 times through

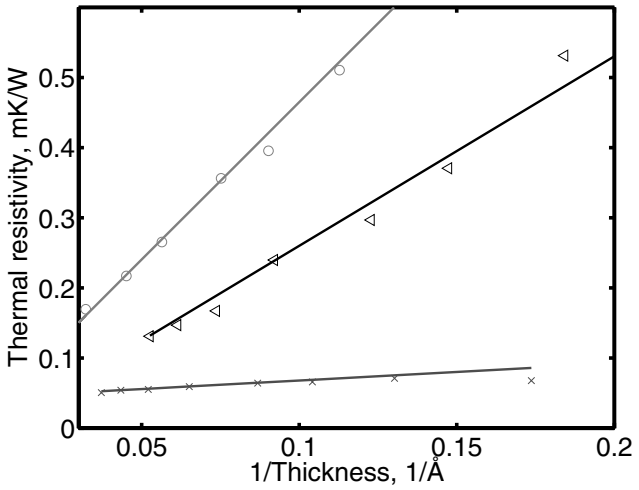

Fig. 6. Thermal resistivity of silicon thin films as calculated with equation (4). The boundary scattering parameters are optimized to reflect the simulated data of Figure 5. Three different free surfaces are present in the six simulation cases: (100)—triangles, $(\bar{1}10)$—crosses, and $(11\bar{2})$—circles. The lines are best fits to the data.

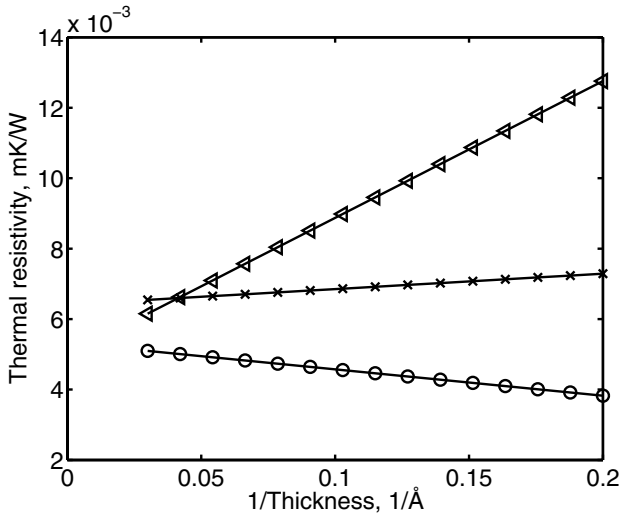

Fig. 7. Results of equation (4) without boundary scattering terms. Group velocity and vibration spectrum are calculated from MD simulations. The free surfaces are: (100) triangles, $(\bar{1}10)$ crosses, and $(\bar{1}\bar{1}\ 2)$ circles.

the system, not four scattering events for each pass. It is noted that the scattering parameter β was the same for all crystal directions, and therefore, the MD data is not exactly reproduced with the optimal scattering parameters for the kinetic theory calculations.

These results clearly prove that phonon boundary scattering on free surfaces is highly anisotropic. In one of the three surfaces studied, surface scattering was nearly specular. Therefore, the in-plane thermal conduction was found to be best in systems with free $(\bar{1}10)$ surfaces. By comparing the results shown in Figures 6 and 5, it can be seen that the kinetic theory results for (100) and $(\bar{1}10)$ surfaces can be optimized quite well. However, for the $(\bar{1}\bar{1}2)$ surface, a significant difference is seen.

4.3 The role of dispersion

As discussed above, the vibrational frequencies of the phonons decrease slightly in thin films. This shows e.g. in the dispersion relation, and therefore changes the group velocity. To analyze the effect these issues have on the resistivity, one can easily exclude the boundary scattering terms, by setting $L_y \to \infty$ and $\alpha \to \infty$ in the relaxation time, equation (8). These results are shown in Figure 7, where a best fit to all cases studied is shown. As seen in the figure, in the cases with free (100) and $(\bar{1}10)$ surfaces, decreasing the size increases the resistivity. In the case of (100) surfaces, phonon confinement effects are included in the dispersion relation, and significant reduction of the group velocity was seen. This increases the thermal resistivity. In addition, in one case with a free $(\bar{1}10)$ surface, phonon confinement was seen. In contrast, in the case of a free $(\bar{1}\bar{1}2)$ surface, only band folding was seen without discrete phonon modes. In the last case, it seems that decreasing the system size with the exclusion of the scattering effects could decrease the resistivity. The reason for this behavior is in the frequency dependent anharmonic scattering term. When the system becomes thinner, the characteristic vibration frequencies decrease, as seen e.g. in the dispersion curves. For the lower frequencies, the anharmonic scattering rates decrease, which decreases the resistivity.

The vibrational spectra for two films is shown in Figure 8. The frequency dependent relaxation times of anharmonic scattering are also depicted. As seen in the figure, the relaxation times increase significantly for frequencies below around 5–10 THz. In this frequency range, the vibrational spectra of thin and thick films are different. The spectrum of thin films is more inclined to the low frequencies, which have longer relaxation times. However, the anharmonic scattering rates, as given by equations (6) and (7), are questionable in nanofilms, where the surface effects start to dominate and change the *anharmonic* interaction between the atoms.

To emphasize, in addition to surface scattering and dispersion, there seems to be a third mechanism affecting the conductivity of thin films: the changes in relaxation times due to the decreasing phonon frequency. The change of the relaxation time due to dispersion has been pointed out, but mainly in terms of the group velocity [26,48], not directly in terms of typical vibrational frequencies. However, it must be noted that in practice, surface scattering, dispersion, and changes in the relaxation times are present simultaneously. In these calculations, decreasing the size always increased the resistivity, indicating that either confinement or surface scattering is the most important factor affecting the thermal resistivity.

The inaccuracy of the potential model for bulk silicon may cast some doubts on the reliability of the results. However, the present potential is known to

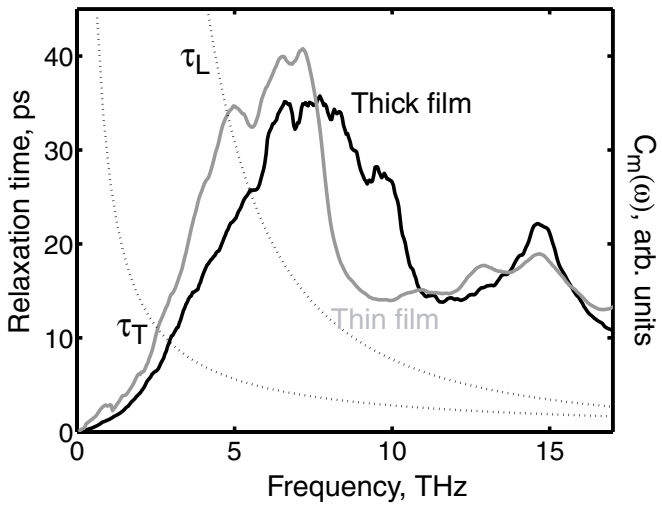

Fig. 8. Density of states in two silicon films. The film thicknesses of the figure are 2 and 0.5 nm. The thicker film is shown with the black line, and the thin film with the grey line. The relaxation times, τ_L and τ_T as calculated respectively with equations (6) and (7) are shown with the dotted lines.

accurately describe the properties of surfaces, and was therefore chosen instead of the commonly used short-range potentials, Stillinger-Weber or Tersoff, even if these potentials are known to describe the bulk dispersion with better accuracy [49]. Moreover, as discussed, the thermal energy is conducted mainly by the low frequency phonons, where the potential was reasonably accurate. As evidence of the accuracy, the kinetic theory with the *calculated* group velocity and density of states gave a very good result compared to the experimental value of conductivity. More complex potentials with larger parameter sets can describe the mechanical (i.e. vibrational) properties of many structures better. At present, probably the most accurate classical potentials for silicon are the EDIP [50] or the empirical multiparameter MEAM [51].

5 Conclusions

This paper addressed the dispersion related thermal resistivity issues in thin films by means of molecular dynamics simulations. Dispersion relations were calculated for both bulk and thin film silicon. The simulations were performed at room temperature, where the characteristic phonon wavelength is only a few lattice constants, and thus the continuum approach for phonons is inapplicable. The interatomic potential used for silicon (MEAM) has previously been used to study silicon surfaces because of its long range of interaction, and was chosen since the free surfaces were expected to play a major role in this study. However, the computations revealed that the MEAM potential does not accurately describe the dispersion of high frequency phonons. The main findings are still expected to be predictive, since the surface properties are well reproduced and phonons with low frequencies carry most heat. The results showed that the dispersion curves remain unfolded even for very thin films. Changes in the dispersion curve became observable only around 2.5 nm. Close to 1.5 nm phonon confinement also became observable, as some of the peaks in the vibration spectrum were split, giving proof of discrete phonon modes.

The thermal conductivities of the films were calculated with non-equilibrium MD, and the results were compared to the kinetic theory predictions. The results were reasonably similar. However, the boundary scattering probability was found to be highly anisotropic. Specifically, in cases with free $(\bar{1}10)$ surfaces, boundary scattering was almost specular. In this case, the thermal resistivity also increased as the film became thinner. The reason for this effect was in the reduced group velocity due to confinement effects. In other cases, boundary scattering was the dominant process for increasing thermal resistivity. In two simulation cases no phonon confinement was seen. In those cases, band folding decreased the characteristic vibrational frequency. Even if band folding could decrease the group velocity, it could simultaneously increase the relaxation time of anharmonic scattering. In these simulations, both these competing mechanisms were, however, negligible as compared to surface scattering or confinement.

This work was funded by the Academy of Finland.

References

1. K.K. Tamma, X. Zhou, J. Thermal Stresses **21**, 405 (1998)
2. D.G. Cahill, W.K. Ford, K.E. Goodson, G.D. Mahan, A. Majumdar, H.J. Maris, R. Merlin, S.R. Phillpot, J. Appl. Phys. **93**, 793 (2003)
3. C.-L. Tien, A. Majumdar, F.M. Gerner, *Microscale energy transport* (Taylor & Francis, 1998)
4. G. Chen, *Nanoscale energy transfer and conversion* (Oxford University Press, 2005)
5. *Microscale and Nanoscale Heat Transfer,* edited by S. Volz (Springer, 2007)
6. P.G. Sverdrup, Y. Sungtaek-Ju, K.E. Goodson, J. Heat Transf. **123**, 130 (2001)
7. S. Mazumder, A. Majumdar, J. Heat Transf. **123**, 749 (2001)
8. D. Lacroix, K. Joulain, D. Lemonnier, Appl. Phys. Lett. **89**, 103104 (2006)
9. R.B. Peterson, J. Heat Transf. **116**, 815 (1994)
10. R.A. Escobar, S.S. Ghai, M.S. Jhon, C.H. Amon, Int. J. Heat Mass Transf. **49**, 97 (2006)
11. G. Chen, Phys. Rev. B **57**, 14958 (1998)
12. M.G. Holland, Phys. Rev. **132**, 2461 (1963)
13. P.K. Schelling, S.R. Phillpot, P. Keblinski, Phys. Rev. B **65**, 144306 (2002)
14. B.C. Daly, H.J. Maris, K. Imamura, S. Tamura, Phys. Rev. B **66**, 024301 (2002)
15. A.J.H. McGaughey, M. Kaviany, Adv. Heat Transf. **39**, 169 (2006)
16. S. Sinha, K.E. Goodson, Int. J. Multiscale Computat. Eng. **3**, 107 (2005)
17. A.J.H. McGaughey, M. Kaviany, Phys. Rev. B **71**, 184305 (2005)
18. A.J.H. McGaughey, M. Kaviany, Int. J. Heat Mass Transf. **47**, 1783 (2004)

19. A.J.H. McGaughey, M. Kaviany, Int. J. Heat Mass Transf. **47**, 1799 (2004)
20. C. Oligschleger, J.C. Schön, Phys. Rev. B **59**, 4125 (1999)
21. S.R. Bickham, J.L. Feldman, Phys. Rev. B **57**, 12234 (1998)
22. Y. Chen, J.R. Lukes, D. Li, J. Yang, Y. Wu, J. Chem. Phys. **120**, 3841 (2004)
23. N. Mingo, Phys. Rev. B **68**, 113308 (2003)
24. J. Shiomi, S. Maruyama, Phys. Rev. B **73**, 205420 (2006)
25. N. Bannov, V. Aristov, V. Mitin, M.A. Stroscio, Phys. Rev. B **51**, 9930 (1995)
26. A. Balandin, K.L. Wang, Phys. Rev. B **58**, 1544 (1998)
27. J. Zou, A. Balandin, J. Appl. Phys. **89**, 2932 (2001)
28. O. Lazarenkova, A. Balandin, Phys. Rev. B **66**, 245319 (2002)
29. M.-J. Huang, T.-M. Chang, W.-Y. Chong, C.-K. Liu, C.-K. Yu, Int. J. Heat Mass Transf. **50**, 67 (2007)
30. P. Heino, Phys. Rev. B **71**, 144302 (2005)
31. M.I. Baskes, Phys. Rev. B **46**, 2727 (1992)
32. N.I. Papanicolau, I.E. Lagaris, G.A. Evangelakis, Surf. Sci. **337**, L819 (1995)
33. P. Heino, E. Ristolainen, Phil. Mag. A **81**, 957 (2000)
34. Y. Fuji, N.A. Lurie, R. Pynn, G. Shirane, Phys. Rev. B **10**, 3647 (1974)
35. P. Jund, R. Jullien, Phys. Rev. B **59**, 13707 (1999)
36. P. Heino, E. Ristolainen, Phys. Scripta **T 114**, 171 (2004)
37. A.J.H. McGaughey, M.I. Hussein, E.S. Landry, M. Kaviany, G.M. Hulbert, Phys. Rev. B **74**, 104304 (2006)
38. M.I. Baskes, Mater. Sci. Eng. A **261**, 165 (1999)
39. M.I. Baskes, Modell. Simul. Mater. Sci. Eng. **5**, 149 (1997)
40. C. Flensburg, R.F. Stewart, Phys. Rev. B **60**, 284 (1999)
41. Z. Li, P. Xiao, in *Proc. 13th International Heat Transfer Conference* (Begell House, Sydney, Australia, 2006), pp. NAN–10
42. C. Dames, G. Chen, J. Appl. Phys. **95**, 682 (2004)
43. P. Gumbsch, M.W. Finnis, Phil. Mag. Lett. **73**, 137 (1996)
44. P. Chantrenne, J.-L. Barrat, J. Heat Transf. **126**, 577 (2004)
45. P. Heino, J. Computat. Theor. Nanosci. **4**, 168 (2007)
46. P.K. Schelling, S.R. Phillpot, P. Keblinski, Appl. Phys. Lett. **80**, 2484 (2002)
47. P. Chantrenne, J.-L. Barrat, X. Blase, J.D. Gale, J. Appl. Phys. **97**, 104318 (2005)
48. A.A. Balandin, IEEE Potent. **2002**, 11 (2002)
49. L.J. Porter, J.F. Justo, S. Yip, J. Appl. Phys. **82**, 5378 (1997)
50. J.F. Justo, M.Z. Bazant, E. Kaxiras, V.V. Bulatov, S. Yip, Phys. Rev. B **58**, 2539 (1998)
51. T.J. Lenosky, B. Sadigh, E. Alonso, V.V. Bulatov, T.D. de la Rubia, J. Kim, A.F. Voter, J.D. Kress, Modell. Simul. Mater. Sci. Eng. **8**, 825 (2000)